Article

Revisiting a Realistic Intersecting D6-Brane with Modified Soft SUSY Terms

Imtiaz Khan [1,2]**, Waqas Ahmed** [3,*]**, Tianjun Li** [1,2] **and Shabbar Raza** [4]

[1] CAS Key Laboratory of Theoretical Physics, Institute of Theoretical Physics, Chinese Academy of Sciences, Beijing 100190, China; ikhan@itp.ac.cn (I.K.); tli@itp.ac.cn (T.L.)
[2] School of Physical Sciences, University of Chinese Academy of Sciences, No. 19A Yuquan Road, Beijing 100049, China
[3] Center for Fundamental Physics and School of Mathematics and Physics, Hubei Polytechnic University, Huangshi 435003, China
[4] Department of Physics, Federal Urdu University of Arts, Science and Technology, Karachi 75300, Pakistan; shabbar.raza@fuuast.edu.pk
* Correspondence: waqasmit@hbpu.edu.cn

Abstract: Because there are a few typos in the supersymmetry-breaking sfermion masses and trilinear soft term, regarding the current Large Hadron Collider (LHC) and dark matter searches, we revisit a three-family Pati–Salam model based on intersecting D6-branes in Type IIA string theory on a $\mathbf{T^6}/(\mathbb{Z_2} \times \mathbb{Z_2})$ orientifold with a realistic phenomenology. We study the viable parameter space and discuss the spectrum consistent with the current LHC Supersymmetry searches and the dark matter relic density bounds from the Planck 2018 data. For the gluinos and first two generations of sfermions, we observe that the gluino mass is in the range [2, 14] TeV, the squarks mass range is [2, 13] TeV and the sleptons mass is in the range [1, 5] TeV. We achieve the cold dark matter relic density consistent with 5σ Planck 2018 bounds via A-funnel and coannihilation channels such as stop–neutralino, stau–neutralino, and chargino–neutralino. Except for a few chargino–neutralino coannihilation solutions, these solutions satisfy current nucleon-neutralino spin-independent and spin-dependent scattering cross-sections and may be probed by future dark matter searches.

Keywords: supersymmetry; D6-brane; dark matter

1. Introduction

In the Large Hadron Collider (LHC), no evidence has been found for physics beyond the Standard Model (SM). The observation of the Higgs boson with mass around m_h = 125 TeV [1,2], whose properties are in good agreement with the SM predictions, poses challenges in the extension of SM, which has been proposed to provide gauge-coupling unification of the electromagnetic, weak, and strong interactions [3–7], a natural explanation of the hierarchy between the electroweak symmetry breaking (EWSB) and Plank scale. One of the promising candidates to deal with the hierarchy problem is supersymmetry (SUSY). The observed Higgs boson mass and null results from SUSY searches of the ATLAS and CMS collaboration have put the low-energy SUSY under stress. Thus, one can consider finding comparatively natural and non-minimal solutions. Besides the hierarchy problem, the promising motivation for physics at the LHC-accessible scale is to explain the observed dark matter (DM) in terms of relic particle density produced in the thermal freeze-out mechanism in the early universe. In the supersymmetric standard models (SSMs) with conserved R-parity, the Lightest Supersymmetric Particle (LSP) is stable and can be the dark matter candidate [8]. According to the recent searches, gluino mass $m_{\tilde{g}} \gtrsim 2.2$ TeV applies for the first two generations of squark mass $m_{\tilde{q}} \gtrsim 2$ TeV [9–11]. In the literature, several interesting scenarios have been recently discussed, particularly the one called "Super-Natural SUSY" [12–14]. In this framework, in the Minimal Supersymmetric Standard Model (MSSM), no residual fine tuning is left in the presence of no-scale

supergravity boundary conditions [15–19] and Giudice–Masiero (GM) mechanism [20] despite a relatively heavy spectrum.

String theory is one of the most promising candidates for quantum gravity. Thus, string phenomenology aims to construct SM or SSMs from the string theory with moduli stabilization and without chiral exotics and try to make unique predictions that can be probed in LHC and other future experiments. In this article, we are interested in updating the phenomenological study of the intersecting D-brane models [21–33]. For the intersecting D-brane model building, the realistic SM fermion Yukawa couplings can be realized only within the Pati–Salam gauge group [34]. Three-family Pati–Salam models have been constructed systematically in Type IIA string theory on the $\mathbf{T^6}/(\mathbb{Z_2} \times \mathbb{Z_2})$ orientifold with intersecting D6-branes [27], and it was found that one model has a realistic phenomenology: the tree-level gauge-coupling unification is realized naturally around the string scale, the Pati–Salam gauge symmetry can be broken down to the SM close to the string scale, the small number of extra chiral exotic states can be decoupled via the Higgs mechanism and strong dynamics, the SM fermion masses and mixing can be accounted for, the low-energy sparticle spectra may potentially be tested at the LHC, and the observed dark matter relic density may be generated for the lightest neutralino as the LSP, and so on [35–37]. In short, as far as we know, this is one of the best globally consistent string models that is phenomenologically viable from the string scale to the EWSB scale.

Because there are a few typos in the supersymmetry-breaking sfermion masses and trilinear soft term, the purpose of this study is to highlight the differences in parameter space associated with the soft SUSY-breaking terms in our previous work [37] and recalculated in [38] with $\mu > 0$. In this work, we display the viable parameter space satisfying the collider and DM bounds along with the Higgs mass bounds. We show that in our present scans, we have A/H-resonance solutions, chargino–neutralino coannihilation, stau–neutralino coannihilation, and stop–neutralino coannihilation. In the case of resonance solutions, $m_{A/H}$ is about 2 TeV or so. In the case of chargino–neutralino coannihilation, the NLSP chargino mass can be between 0.7 TeV to 2.3 TeV and the NLSP stau is in the mass range of 0.2 TeV to 1.8 TeV. As far as the NLSP stop solutions are concerned we have solutions from 0.15 TeV to 0.9 TeV. Most of the parameter space related to this scenario has already been probed by the LHC SUSY searches. It should also be noted that the above-mentioned solutions, except for some of the chargino–neutralino solutions, are consistent with the ongoing and future astrophysical dark matter experiments.

This paper is organized as follows. In Section 2 we highlight the model's features related to our study. In Section 3 we review the detail of the range of values we employed and the phenomenological constraints we impose. We discuss the numerical results of our scanning in Section 4. Section 5 gives a summary and conclusion.

2. The Realistic Pati–Salam Model from the Intersecting D6-Branes Compatified on a $\mathbf{T^6}/(\mathbb{Z_2} \times \mathbb{Z_2})$ Orientifold

We are going to focus on the realistic intersecting D6-brane model [27] with modified soft SUSY terms calculated in [38]. Ignoring the CP-violating phase, the SSB terms by nonzero F-terms of the dilaton F^S and three complex structure moduli F^{U^i}, where $i = 1, 2, 3$ can be parametrized by the $\Theta_1, \Theta_2, \Theta_3, \Theta_4$ and the gravitino mass $m_{3/2}$. Here, $\Theta_4 \equiv \Theta_S$ applies for the dilaton case. The relationship between the Θ's is given as [37]

$$\sum_{i=1}^{4} \Theta_i^2 = 1. \tag{1}$$

The SSB terms at the grand unification (GUT) scale in terms of these parameters can be written as [38]

$$M_1 = m_{3/2}(0.519615\Theta_1 + 0.34641\Theta_2 + 0.866025\Theta_3),$$

$$M_2 = m_{3/2}(0.866025\Theta_2 - 0.866025\Theta_4),$$

$$M_3 = m_{3/2}(0.866025\Theta_2 + 0.866025\Theta_3),$$

$$A_0 = m_{3/2}(-0.292797\Theta_1 - 1.43925\Theta_2 - 0.573228\Theta_3 + 0.573228\Theta_4),$$

$$\widetilde{m}_L^2 = m_{3/2}{}^2\Big(1 - 2.02977\Theta_1{}^2 + 0.75\Theta_1\Theta_2 - 1.5\Theta_1\Theta_4 - 0.0440466\Theta_2{}^2 - 1.5\Theta_2\Theta_3$$
$$+ 0.286907\Theta_3{}^2 + 0.75\Theta_3\Theta_4 + 0.286907\Theta_4{}^2\Big),$$

$$\widetilde{m}_R^2 = m_{3/2}{}^2\Big(1 - 0.0880932\Theta_1{}^2 - 1.5\Theta_1\Theta_2 + 0.75\Theta_1\Theta_3 + 0.75\Theta_1\Theta_4 - 0.0880932\Theta_2{}^2$$
$$+ 0.75\Theta_2\Theta_3 + 0.75\Theta_2\Theta_4 - 0.419047\Theta_3{}^2 - 1.5\Theta_3\Theta_4 - 2.40477\Theta_4{}^2\Big),$$

$$\widetilde{m}_{H_u}^2 = \widetilde{m}_{H_d}^2 = m_{3/2}^2(1.0 - (1.5\Theta_3^2) - (1.5\Theta_4^2)). \tag{2}$$

All the above results are subject to the constraint in Equation (1). Here, $M_{1,2,3}$ are the gauginos masses for the gauge groups $U(1)_Y$, $SU(2)_L$, $SU(3)_c$, respectively, A_0 is a common trilinear scalar coupling term and $\widetilde{m}_L$ and $\widetilde{m}_R$ are the soft mass terms for the left-handed and right-handed squarks and sleptons, respectively, and $\widetilde{m}_{H_{u,d}}$ are the SSB Higgs soft mass terms. The gauginos and Higgs soft masses are the same as in the case [37]. The trilinear coupling $A0$ equation is different only by the coefficients of Θ's with no new extra terms, unlike the case of $\widetilde{m}_L{}^2$ and $\widetilde{m}_R{}^2$. In the left-handed squarks soft mass square term $\widetilde{m}_L{}^2$ in Equation (2), apart from the coefficients of Θ's we have some additional terms such as $\Theta_1\Theta_4$ and $\Theta_2\Theta_3$. Similarly, the right-handed sleptons soft mass square term $\widetilde{m}_R{}^2$ irrespective of the coefficients of Θ's; we also have some additional new terms such as $\Theta_1\Theta_3$, $\Theta_1\Theta_4$, $\Theta_2\Theta_3$, and $\Theta_2\Theta_4$[1]. These terms predict that our parameters space differs from the previously discussed results [37], and the details are discussed in Section 4.

3. Scanning Procedure and Phenomenological Constraints

We employ the ISAJET 7.85 package [39] to perform random scans over the parameter space of the above-presented intersecting D6-brane model. Following [37], we can parametrize the three independent Θ_i with $i = 1, 2, 3$ that enter the soft masses in (2) in terms of γ_1, γ_2, and Θ_4 as,

$$\Theta_1 = \cos(\beta)\cos(\alpha)\sqrt{1 - \Theta_4^2},$$

$$\Theta_2 = \cos(\beta)\sin(\alpha)\sqrt{1 - \Theta_4^2},$$

$$\Theta_3 = \sin(\beta)\sqrt{1 - \Theta_4^2},$$

$$\text{where}\quad \alpha \equiv 2\pi\gamma_1,\ \beta \equiv 2\pi\gamma_2. \tag{3}$$

We perform random scans over the following ranges of the model parameters:

$$0 \leq \gamma_1 \leq 1\,,$$
$$0 \leq \gamma_2 \leq 1\,,$$
$$0 \leq \Theta_4 \leq 1\,,$$
$$0 \leq m_{3/2} \leq 15\ \text{TeV}\,,$$
$$2 \leq \tan\beta \leq 60\,, \tag{4}$$

where $\tan\beta$ is the ratio of vacuum expectation values (VEVs) of the Higgs fields. We use the $m_t = 173.3$ GeV [40]. We employ the Metropolis–Hastings algorithm as described in [41,42]. We have done our scans with $\mu > 0$ and collected the data points that satisfy the requirement of a successful radiative EWSB (REWSB). Besides, we have also selected those

points, with the lightest neutralino being the LSP. After collecting the data, we impose the following constraints that the LEP2 experiment set on charged sparticles masses [43]

$$m_{\tilde{t}_1}, m_{\tilde{b}_1} \gtrsim 100 \text{ GeV} , \tag{5}$$

$$m_{\tilde{\tau}_1} \gtrsim 105 \text{ GeV} , \tag{6}$$

$$m_{\tilde{\chi}_1^\pm} \gtrsim 103 \text{ GeV} , \tag{7}$$

and the combined Higgs mass reported by the ATLAS and CMS collaborations [44]

$$m_h = 125.09 \pm 0.21 (\text{stat.}) \pm 0.11 (\text{syst.}) \text{ GeV}. \tag{8}$$

Because of the theoretical uncertainty in the calculation of m_h, we consider the following range for the Higgs mass [45,46]

$$122 \text{ GeV} \leq m_h \leq 128 \text{ GeV}. \tag{9}$$

Furthermore, we use the IsaTools package [47–51] to implement the following observables B-physics constraints [52,53]:

$$1.6 \times 10^{-9} \leq \text{ BR}(B_s \rightarrow \mu^+ \mu^-) \leq 4.2 \times 10^{-9} \quad , \tag{10}$$

$$2.99 \times 10^{-4} \leq \text{ BR}(b \rightarrow s\gamma) \leq 3.87 \times 10^{-4} \quad , \tag{11}$$

$$0.70 \times 10^{-4} \leq \text{ BR}(B_u \rightarrow \tau\nu_\tau) \leq 1.5 \times 10^{-4} \quad . \tag{12}$$

In addition to the above constraints, we consider the following conditions on the gluino and first/second-generation squarks masses from the LHC and Planck bound based on [9–11,54]

$$m_{\tilde{g}} \gtrsim 2.2 \text{ TeV (for } m_{\tilde{q}} \gtrsim 2) \text{ TeV}$$
$$0.114 \leq \Omega_{\tilde{\mathcal{O}}_1^0} h^2 (\text{Planck}) \leq 0.126 \tag{13}$$

4. Numerical Results and Discussion

In Figure 1, we show graphs for various parameters in Equation (3). We consider $\mu > 0$ and the color coding is as follows. Grey points satisfy the REWSB and yield LSP neutralino. Blue points satisfy LEP, Higgs mass bound, B-physics, and LHC sparticle mass bounds. Red points form a subset of blue points and satisfy Planck 2018 bounds on cold dark matter relic density within 5σ.

In our scanning, we see in the Θ_1-Θ_2 plane, the range of the red points for Θ_1 is $-0.9 \lesssim \Theta_1 \lesssim 0.7$, but most of the points are concentrated from -0.4 to 0.7, while for Θ_2 it is $-0.9 \lesssim \Theta_2 \lesssim 0.8$. Also, for Θ_2 most of the points are concentrated from 0.3 to 0.8 and -0.8 to -0.4. For Θ_1 and Θ_2, we have red point solutions almost everywhere in the entire range except for the Θ_2 where the solutions are in the -0.4 to 0.3 range. On the other hand, blue points are more or less everywhere in the plot. In Θ_1-Θ_3 plane, the concentration of red points favors the positive range as in the case of Θ_1-Θ_2 plane. We also see a small concentration of red points in the negative range for the small negative value of Θ_1 and for the large negative value of Θ_3. Blue points are almost everywhere in the plot in contrast to the Θ_1-Θ_2 plane, as we have the density of points around the center of the plot. In the Θ_3-Θ_2 plane, here again, we see the concentration of red points favors the positive range for Θ_2 and Θ_3. But we also see a small concentration of red points in the negative range smaller than that of the positive range for a small negative value of Θ_2 and a large negative value of Θ_3. For all points, we see a polarization-like pattern compared to other planes and having no points in the center of the plot.
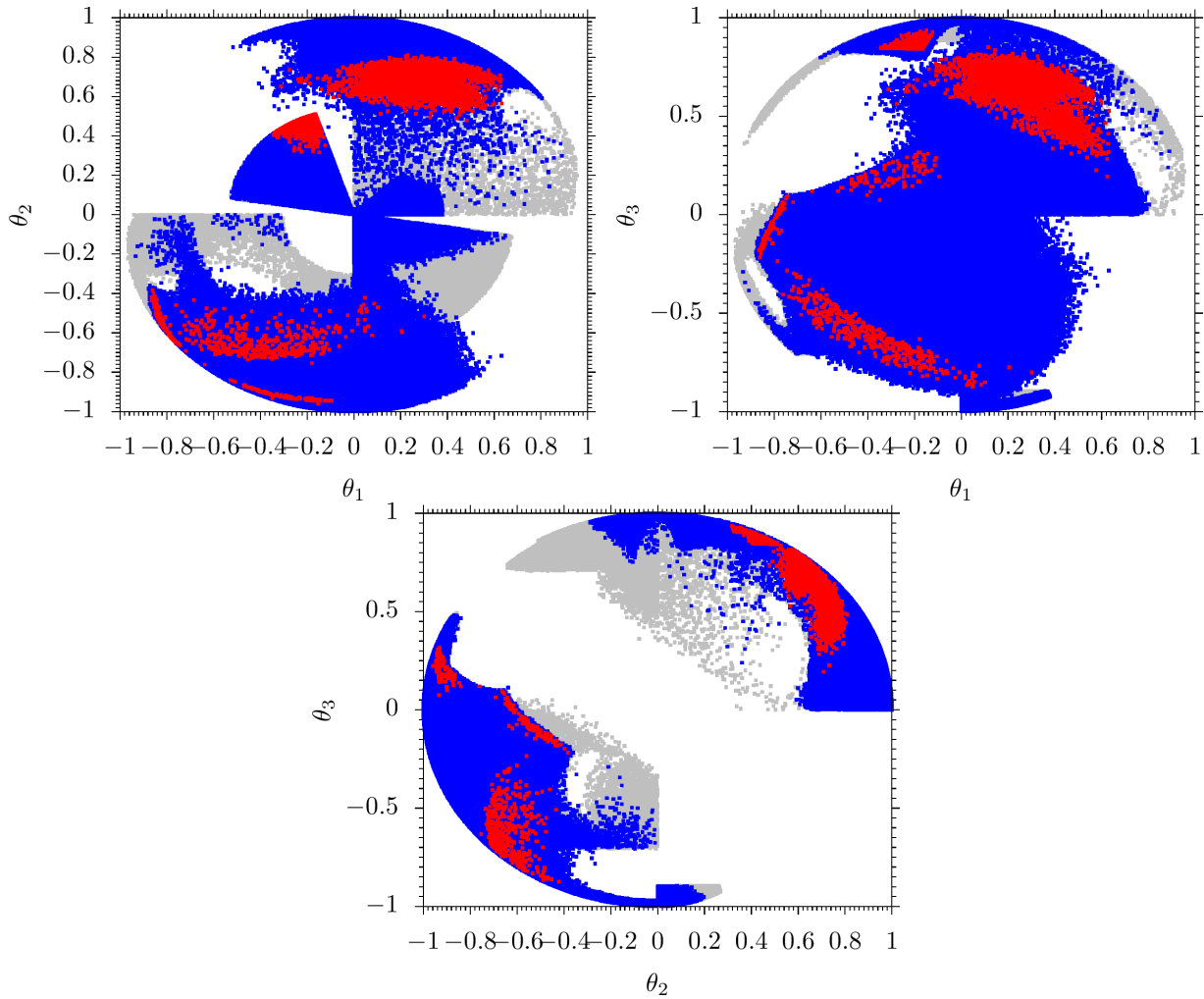
Figure 1. Grey points satisfy the REWSB and yield LSP neutralinos. The blue points are the subset of gray points that satisfy the LEP bound, Higgs mass bound, B-physics, and LHC sparticle mass bounds. Red points are a subset of blue points that satisfy 5σ Planck relic density bounds.

We calculate the (SSB) parameters given in Equation (2). We present the results in Figures 2 and 3, color coding is the same as that of Figure 1. We present the M_1–M_2 plane in the top left panel. Red points are in the range from $[-5, 6]$ TeV for M_1, but the large density favors the positive range from $[4, 6]$ TeV. The density of red points smaller than that of the positive range was also concentrated for the negative values $[-5, -2]$ TeV for M_1. For the blue points, we have solutions almost everywhere for M_1 from $[-5, 6]$ TeV except around 1 TeV. We also see the concentration of red points at $[1, 3]$ TeV in the positive range and $[-3.5, -1]$ TeV in the negative range for M_2. For the blue points, we have solutions almost everywhere from $[-5, 4.5]$ TeV for M_2. In short, we see a polarisation kind of pattern for red and blue points having no points in the center. We present the M_2–M_3 plane in the top right panel. We see almost a similar pattern to that of the M_1–M_2 plane but a slight difference can be observed in that the red points are concentrated at $[2, 3]$ TeV and $[-3.5, -2]$ TeV for M_2, and at $[4, 7]$ TeV and $[-2, -6]$ TeV for M_3. For blue points, we have solutions for M_2 everywhere from $[-5, 4.5]$ TeV, and for M_3, $[-6, 7.5]$ TeV except in the middle. In short, for all the points, we again see a similar pattern as that of the M_1–M_2 plane. Finally, we see the M_1–M_3 plot in the bottom panel. Similar to the two gaugino plots, here too we see a similar polarization pattern in solutions. The only difference is that since the ranges of M_1 and M_3 are relatively larger than M_2, the plot in M_1–M_3 looks slim.
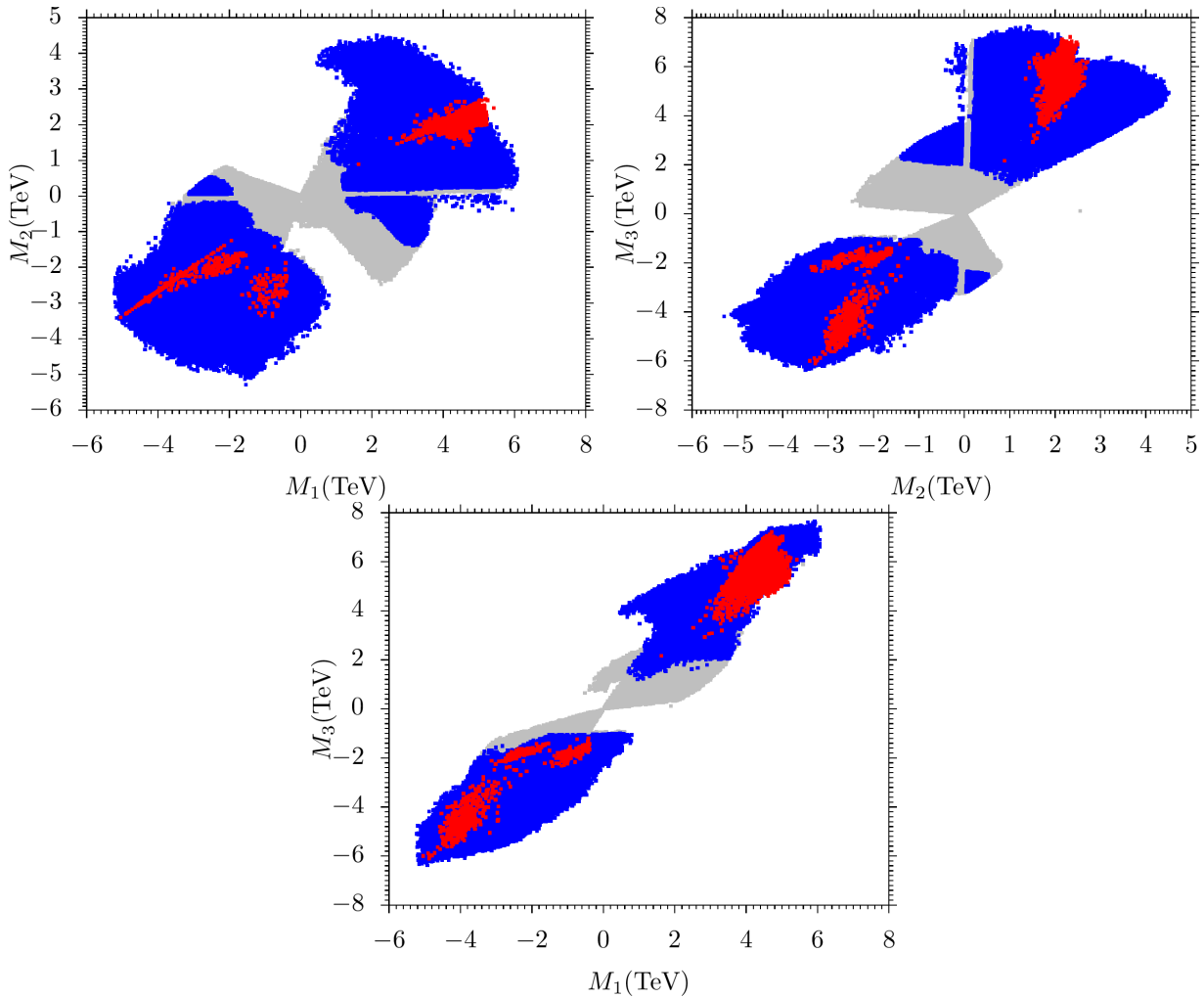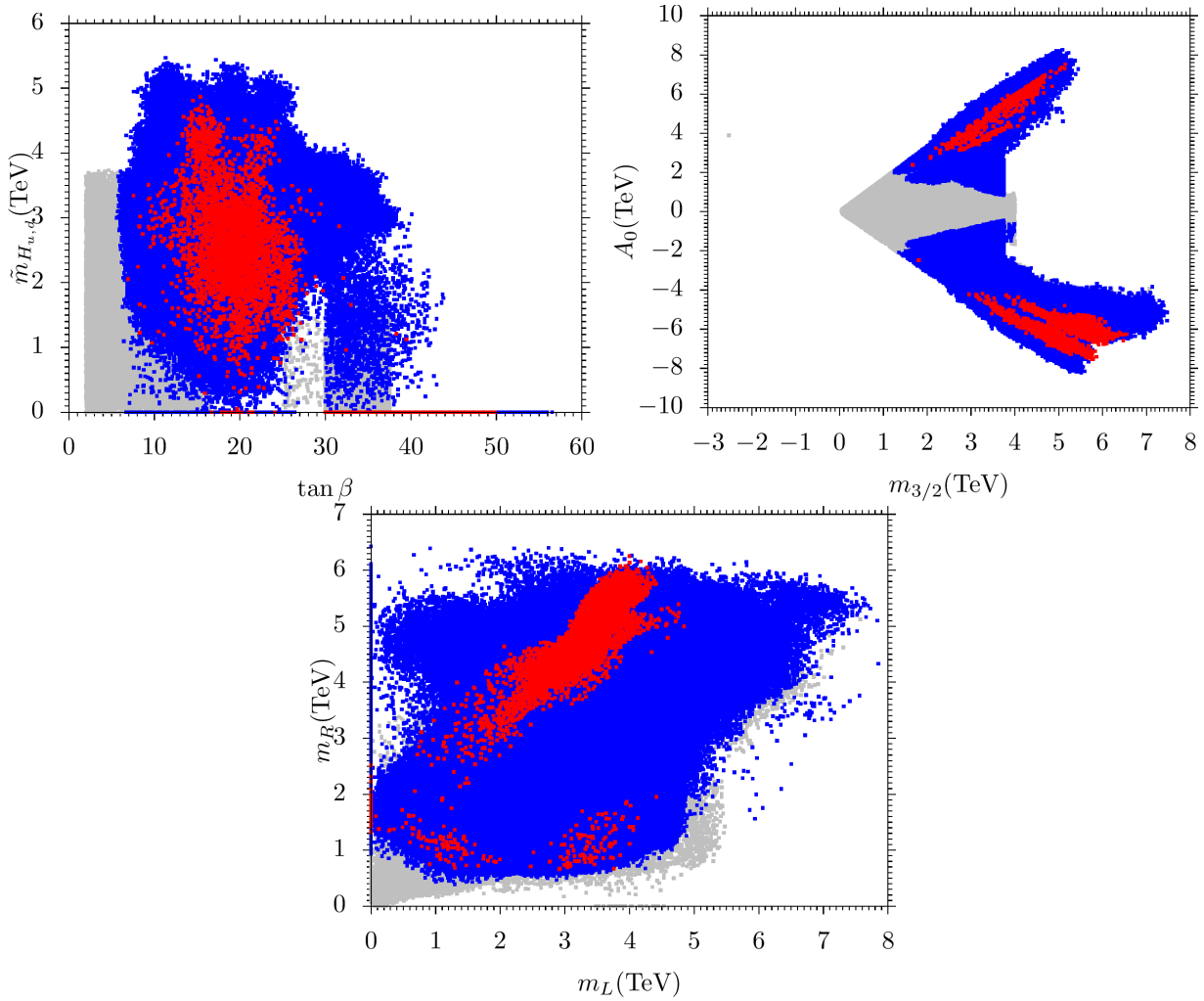
Figure 2. Plots of results in M_1–M_2, M_1–M_3, and M_3–M_2 planes. The color coding and the panel description are the same as in Figure 1.

In Figure 3, we present the $\tan\beta$–$\widetilde{m}_{H_{u,d}}$, $m_{3/2}$–A_0, and $\widetilde{m}_L$–$\widetilde{m}_R$ planes. Color coding is the same as in Figure 1. In the $\tan\beta - \widetilde{m}_{H_{u,d}}$ plane, we see that the red points solution is $7 \lesssim \tan\beta \lesssim 50$ with $0 \lesssim \widetilde{m}_{H_{u,d}} \lesssim 5$ TeV but most of the points concentrate in the range $\tan\beta = 15$ to $\tan\beta = 25$. For blue points, we have a solution for $6.5 \lesssim \tan\beta \lesssim 57$ and $0 \lesssim \widetilde{m}_{H_{u,d}} \lesssim 5.4$ TeV. In the $m_{3/2} - A_0$ plane, most of the red points concentrate in the range $[2, 7]$ TeV for $m_{3/2}$ and $|4|$ TeV to $|8|$ TeV for A_0. But it can be seen that red solutions favor $A_0 < 0$.

In the $\widetilde{m}_L$–$\widetilde{m}_R$ plane we see most of the concentrations of red points at $[2, 4.5]$ TeV for $\widetilde{m}_L$ and at $[3, 6]$ TeV for $\widetilde{m}_R$. For the blue points, we have solutions almost everywhere from $[0, 7.9]$ TeV for $\widetilde{m}_L$ and from $[0.5, 6.5]$ TeV for $\widetilde{m}_R$.

In Figure 4 we present $m_{\tilde{t}_1}$–$m_{\tilde{g}}$ and m_h–μ planes. The panel description and color coding are the same as in Figure 1. As we know LHC is a color particle machine and among the color sparticles, gluinos are the smoking guns for SUSY signals. As we have seen before we have heavy M_3 and also relatively heavy left-handed and right-handed scalars, consequentially we have heavy gluinos and stops. For both red and blue points, gluino mass is in the range of 2.2 TeV to 15 TeV, and stop mass $m_{\tilde{t}_1}$ is from 0.1 TeV to 11 TeV. It should be noted that at the 100 TeV pp collider with $30\,ab^{-1}$ integrated luminosity, gluino ($\tilde{g}$) mass can be probed up to 11 TeV and 17 TeV via heavy flavor decays and via light flavor decays, respectively, and stop ($\tilde{t}_1$) mass up to 11 TeV can be discovered [55–58]. In the right panel, we display the plot in the m_h–μ plane. Here we see that both red and blue points are in the range $[0.8, 9]$ TeV. This implies that we have heavier higgsinos.

Figure 3. Plots in $\tan\beta$–$\widetilde{m}_{H_{u,d}}$, $A_0 - m_{3/2}$, and $\widetilde{m}_L$–$\widetilde{m}_R$ planes. The color coding and the panel description are the same as in Figure 1.
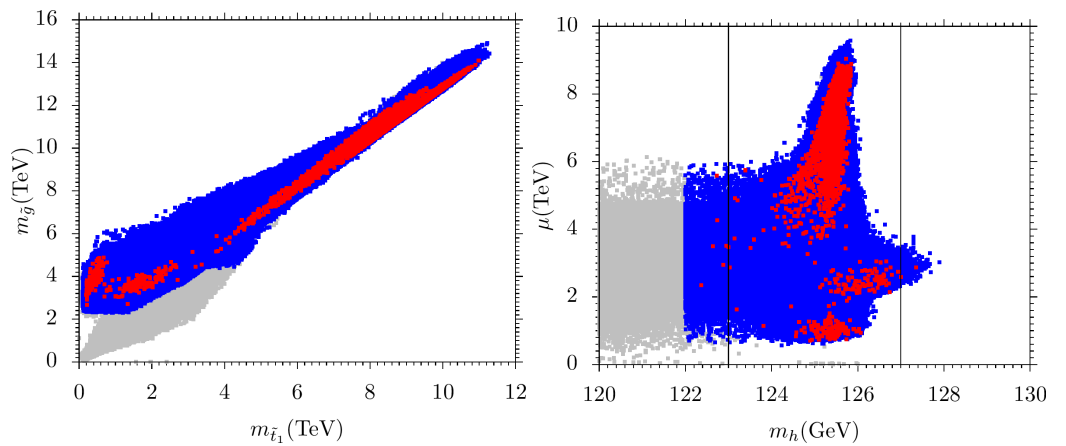
Figure 4. Plots of results in $\widetilde{t}_1 - m_{\widehat{g}}$ and $m_h - \mu$ planes. The color coding and the panel description are the same as in Figure 1.

We now present results with the LSP neutralino mass and the masses of other particles of our model that are possibly light, i.e., $\widetilde{\tau}_1$, A, $\widetilde{\chi}_1^{\pm}$, and $\widetilde{t}_1$ masses in Figure 5. The description and color coding are the same as in Figure 1. The solid black lines show the mass degeneracy between the listed particles and for $m_{\widetilde{\chi}_1^0} - m_A$ plane, indicates the $m_A = 2m_{\widetilde{\chi}^0}$ region. In the top left panel, we present a plot in the $m_{\widetilde{\chi}_1^0} - m_A$ plane. We see that there are a couple

of red points that have $m_A > 2$ TeV. In this scenario, correct relic density is achieved when a pair of LSP neutralinos annihilates into a CP-odd Higgs. It should be noted that for $m_A \lesssim 1.7$ TeV is excluded for $\tan\beta \lesssim 30$ [59]. In addition to it at Run 2, Run 3, and HL-LHC the CP-odd Higgs A with $\tan\beta \lesssim 10$ can be excluded for masses 1 TeV, 1.1 TeV, and 1.4 TeV, respectively. We hope that future research will be able to investigate such solutions [60,61].
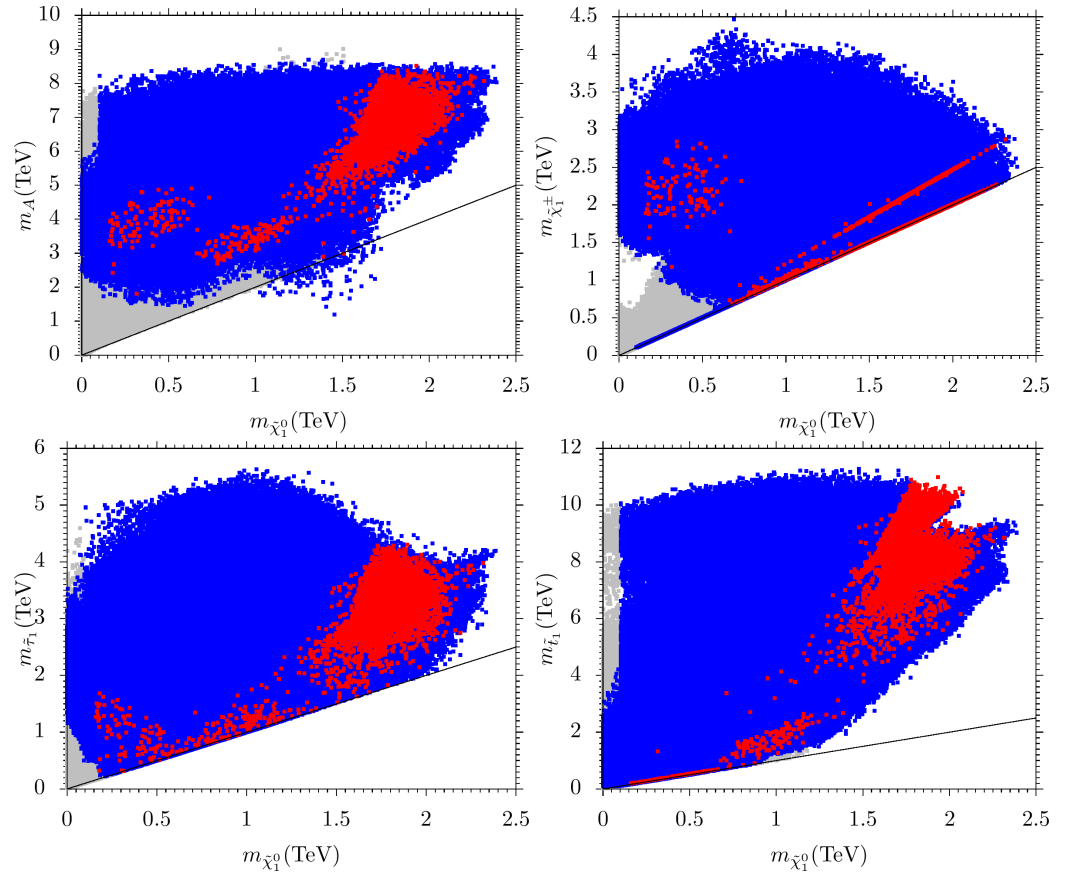
Figure 5. Plots in $m_{\tilde{\chi}_1^0}-m_A$, $m_{\tilde{\chi}_1^0}-m_{\tilde{\chi}_1^\pm}$, $m_{\tilde{\chi}_1^0}-m_{\tilde{\tau}_1}$ and $m_{\tilde{\chi}_1^0}-m_{\tilde{t}_1}$ planes. Color coding and panel description are the same as in Figure 1.

In the top right panel, we show a plot in the $m_{\tilde{\chi}_1^0} - m_{\tilde{\chi}_1^\pm}$ plane. If we do not care about Planck2018 relic density bounds, we have a neutralino and chargino degenerate masses solution from [0.1, 2.4] TeV but the degenerate masses solution is compatible with Planck2018 bounds from [0.7, 2.3] TeV range. The Ref. [62] has reported the 95% exclusion for sleptons as well as SM-boson-mediated decays of $\tilde{\chi}_1^+ \tilde{\chi}_1^+$ and $\tilde{\chi}_1^\pm \tilde{\chi}_2^0$. It can be seen that the charginos heavier than 300 GeV are safe when they are mass-degenerate with the LSP neutralino. On the other hand in the parameter space where slepton masses are heavier than charginos, these slepton-mediated decays will not take place. Since we also have heavier NLSP chargino solutions, we hope that such solutions will be probed in future LHC searches. In the lower left panel, we present the plot in the $m_{\tilde{\chi}^0} - m_{\tilde{\tau}_1}$ plane. Here, we observe that the range of red points where $\tilde{\tau}_1$ is nearly degenerate with $m_{\tilde{\chi}^0}$ is from [0.3, 1.8] TeV but for the blue points the mass degeneracy ranges are from [0.15, 2.1] TeV. Thus we note that our solutions are consistent with the results reported in [63] with 137 fb^{-1} at 13 TeV.

In the lower left panel we present the plot in the $m_{\tilde{\chi}^0} - m_{\tilde{t}_1}$ plane. Here we have red points 0.2 TeV $\lesssim m_{\tilde{t}_1} \lesssim 0.9$ TeV along the solid line. Such solutions represent scenarios where NLSP stop is mass-degenerate with the LSP neutralino. In such a case , $\tilde{t}_1 \to c\tilde{\chi}_1^0$ is the dominant decay channel. From the latest study [64], it is evident that in such a scenario the stop mass around 600 GeV has been excluded [65]. Thus, nearly half of our

solutions have already been excluded. We anticipate that future studies will investigate the remaining NLSP stop solution in a small mass gap region.

In Figure 6, we present the plots for spin-independent (left) and spin-dependent (right) neutralino–proton scattering cross-section vs. the neutralino mass. We consider the impact of current and future dark matter (DM) searches on our model. In the left panel, the solid black and yellow lines represent the current LUX [66] and XENON1T [67,68] bounds, respectively, whereas the green and red lines depict the projection of future limits [69] of XENON1T with 2 $t \cdot y$ exposure and XENONnT with 20 $t \cdot y$ exposure, respectively. In the right panel, the solid black line represents the current LUX bound [70], the orange line represents the future Lux–Zeplin (LZ) bound [71] and the blue line represents the IceCube DeepCore [72]. It can be seen that most points are consistent with current LUX and XENON1T bounds. Some points will also be investigated by future Xenon experiments. On the other hand, there are some points that are excluded by the current LUX and Xenon1T experiments. Such points represent the scenario where the chargino is the NLSP and the LSP neutralino is bino-higgsino mixed dark matter. We also want to make a comment here that our NLSP stop solutions are constrained by the collider searches below 600 GeV and the remaining solutions are constrained by the LUX and Xenon experiments. We note that points with NLSP mass around 900 GeV (which is the heaviest NLSP stop in our model) have $\sigma^{SI}(\chi, p)$ just below the current LUX and Xenon1T bounds. Thus future DM searches will definitely investigate such solutions.
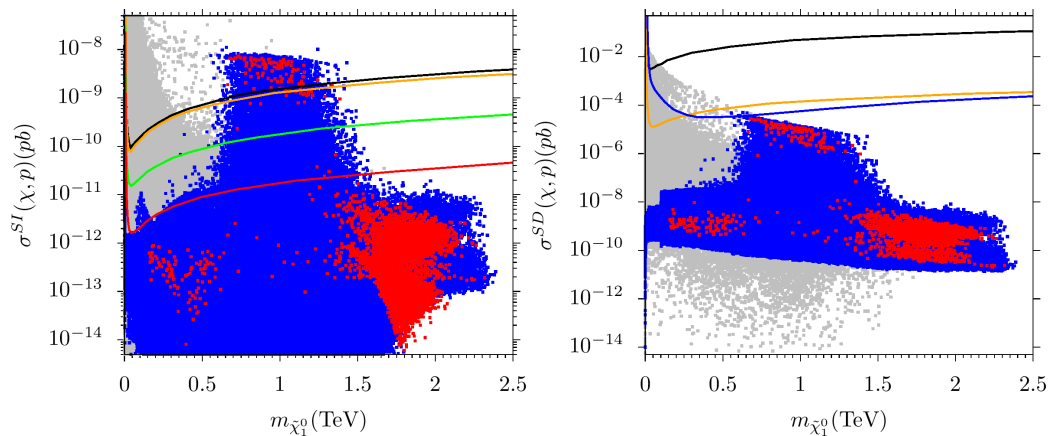
Figure 6. The spin-independent (**left**) and spin-dependent (**right**) neutralino–proton scattering cross-section vs. the neutralino mass. In the left panel, the solid black and orange lines depict the current LUX [66] and XENON1T [67,68] bounds, and the solid green and red lines show the projection of future limits [69] of XENON1T with 2 $t \cdot y$ exposure and XENONnT with 20 $t \cdot y$ exposure, respectively. In the right panel, the black solid line is the current LUX bound [70], the blue solid line represents the IceCube DeepCore [72], and the orange line shows the future LZ bound [71]. The color code in the description is the same as in the Figure 1.

In the right panel, the black solid line represents the current LUX bound [70], the orange line represents the future Lux–Zeplin (LZ) bound [71] and the blue line represents the IceCube DeepCore [72]. Here we see that all solutions are consistent with current and future dark matter searches.

To be specific, we also present a table of benchmark points from our data which explain the various scenarios of our discussion. In Table 1, all points satisfy the constraints described in Section 3, and masses are given in GeV. Point 1 is an example of a chargino–neutralino coannihilation scenario. Here $m_{\tilde{\chi}_1^0} = 0.711$ TeV and $m_{\tilde{\chi}_1^\pm} = 0.724$ TeV. Point 2 shows a stop–neutralino case where $m_{\tilde{\chi}_1^0} = 0.876$ TeV and $m_{\tilde{\chi}_1^\pm} = 0.911$ TeV. Point 3 represents A/H resonance solutions with $m_A(m_H) = 2900$ GeV (2919 GeV). Finally, point 3 displays a stau–neutralino scenario with $m_{\tilde{\chi}_1^0} = 0.807$ TeV and $m_{\tilde{\chi}_1^\pm} = 0.821$ TeV. We also note that point 2 and point 4 have $\mu \lesssim 1$ TeV which means these are relatively less fine-tuned solutions.

Table 1. All quantities with mass dimension are in the unit of GeV and $\mu > 0$. All points satisfy the particle mass bounds, B-physics constraints, and Planck bounds described in Section 3. Point 1 represents chargino–neutralino coannihilation while point 2 represents neutralino–stop coannihilations. Point 3 depicts *A*-resonance; and finally, point 4 displays neutralino–stau coannihilation.

	Point 1	Point 2	Point 3	Point 4
$\widetilde{m}_L$	1242.9	1931.8	1779.7	905.2
$\widetilde{m}_R$	1748.8	787.7	4152	748.2
M_1	1630.2	-1989.9	-2943.9	-1871.1
M_2	887.3	-2120.4	-2256.8	-1713.6
M_3	2164.8	-1796.9	-4523.8	-1421.3
A_0	-2475.7	4032.3	4920.8	3151.6
$\tan\beta$	16.3	12	39.5	16.9
$\widetilde{m}_{H_u} = \widetilde{m}_{H_d}$	987	3481	1122.3	2634.9
μ	2944.2	999.7	5797	859
m_h	122.8	125.7	125.4	125.1
m_H	3064	3804	2919	2842
m_A	3044	3779	2900	2823
$m_{H^\pm}$	3065	3805	2921	2843
$m_{\widetilde{\chi}^0_{1,2}}$	711, -724	876, -1015	1388, 1694	807, -873
$m_{\widetilde{\chi}^0_{3,4}}$	2954, -2955	-1015, 1763	-5786, 5787	897, 1413
$m_{\widetilde{\chi}^\pm_{1,2}}$	724, 2958	985, 1738	1698, 5783	838, 1398
$m_{\widetilde{g}}$	4546	3810	8888	3049
$m_{\widetilde{u}_{L,R}}$	4096, 4284	3994, 3366	7874, 8552	2967, 2763
$m_{\widetilde{t}_{1,2}}$	3376, 3693	911, 3237	6428, 7095	1164, 2346
$m_{\widetilde{d}_{L,R}}$	4097, 4274	3343, 3995	7875, 8536	2968, 2739
$m_{\widetilde{b}_{1,2}}$	3656, 3693	3234, 3283	6496, 7416	2362, 2604
$m_{\widetilde{\nu}_{1,2}}$	1380	2369	2559	1450
$m_{\widetilde{\nu}_3}$	1338	2336	2258	1383
$m_{\widetilde{e}_{L,R}}$	1386, 1847	2370, 1064	2550, 4133	1455, 1017
$m_{\widetilde{\tau}_{1,2}}$	1342, 1784	912, 2338	2554, 3732	821, 1390
σ_{SI}(pb)	2.56×10^{-12}	7.52×10^{-10}	2.88×10^{-13}	3.84×10^{-9}
σ_{SD}(pb)	2.17×10^{-9}	1.98×10^{-6}	7.60×10^{-11}	1.1×10^{-5}
$\Omega_{CDM}h^2$	0.119	0.119	0.117	0.114

5. Summary and Conclusions

Because there are a few typos in the supersymmetry-breaking sfermion masses and trilinear soft term, we revisit the phenomenological survey of the intersecting D-brane model with modified soft SUSY terms, focused on the LHC and DM constraints, and predict low-energy SUSY particle spectra. The three-family Pati–Salam models have been constructed systematically in Type IIA string theory on the $\mathbf{T^6}/(\mathbb{Z}_2 \times \mathbb{Z}_2)$ orientifold with intersecting D6-branes [27]. Our phenomenological survey of this three-family Pati–Salam model has been presented in detail in Section 4. In this work, we display the viable parameter space satisfying the collider and DM bounds along with the Higgs mass bounds. We show that in our present scans, we have A/H-resonance solutions, chargino–neutralino coannihilation, stau–neutralino coannihilation, and stop–neutralino coannihilation. In the case of resonance solutions, $m_{A/H}$ is about 2 TeV or so. In the case of chargino–neutralino coannihilation, the NLSP chargino mass can be between 0.7 TeV to 2.3 TeV and the NLSP stau is in the mass range of 0.2 TeV to 1.8 TeV. As far as the NLSP stop solutions are concerned we we have solutions from 0.15 TeV to 0.9 TeV. Most of the parameter space related to this scenario has already been probed by the LHC SUSY searches. It should also be noted that the above-mentioned solutions, except for some of the chargino–neutralino solutions, are consistent with the ongoing and future astrophysical dark matter experiments.

Data Availability Statement: Data are contained within the article.

Conflicts of Interest: The authors declare no conflicts of interest.

Note

[1] The gaugino masses are almost squeezed up to 50% from the previous study, which provided an important contribution in evaluating the sparticle masses from the GUT to electroweak scale in SUSY GUTs. Similarly, the spectrum for $\widetilde{m}_R{}^2$, $\widetilde{m}_L{}^2$, $\widetilde{m}_{H_{u,d}}$, and A_0 in the negative range are also squeezed up to 50% in our new study. In short, the overall mass spectrum is squeezed from 20% to 50%. Furthermore, we are unable to have the gluino coannihilation channel in our new results, and previously we were expecting to have some points that are important regarding LHC SUSY searches. We have no stop coannihilation in the previous study and in the new study there is stop coannihilation up to 1 TeV for the Planck2018 relic density (within 5σ) satisfied points. Similarly, we have no stau coannihilation points below 1 TeV consistent with the Planck20018 relic density bounds within 5σ and in the new study, there is stau coannihilation below 1 TeV.

References

1. Aad, G.; Abajyan, T.; Abbott, B.; Abdallah, J.; Khalek, S.A.; Abdelalim, A.A.; Aben, R.; Abi, B.; Abolins, M.; AbouZeid, O.S.; et al. Observation of a new particle in the search for the Standard Model Higgs boson with the ATLAS detector at the LHC. *Phys. Lett. B* **2012**, *716*, 1–29.
2. Chatrchyan, S.; Khachatryan, V.; Sirunyan, A.M.; Tumasyan, A.; Adam, W.; Aguilo, E.; Bergauer, T.; Dragicevic, M.; Erö, J.; Fabjan, C.; et al. Observation of a new boson at a mass of 125 GeV with the CMS experiment at the LHC. *Phys. Lett. B* **2012**, *716*, 30–61.
3. Dimopoulos, S.; Raby, S.; Wilczek, F. Supersymmetry and the Scale of Unification. *Phys. Rev. D* **1981**, *24*, 1681. [CrossRef]
4. Marciano, W.J.; Senjanovic, G. Predictions of Supersymmetric Grand Unified Theories. *Phys. Rev. D* **1982**, *25*, 3092. [CrossRef]
5. Amaldi, U.; de Boer, W.; Furstenau, H. Comparison of grand unified theories with electroweak and strong coupling constants measured at LEP. *Phys. Lett. B* **1991**, *260*, 447. [CrossRef]
6. Ellis, J.R.; Kelley, S.; Nanopoulos, D.V. Probing the desert using gauge coupling unification. *Phys. Lett. B* **1991**, *260*, 131. [CrossRef]
7. Langacker, P.; Luo, M.X. Implications of precision electroweak experiments for M_t, ρ_0, $\sin^2 \theta_W$ and grand unification. *Phys. Rev. D* **1991**, *44*, 817. [CrossRef]
8. Jungman, G.; Kamionkowski, M.; Griest, K. Supersymmetric Dark Matter. *Phys. Rept.* **1996**, *267*, 195. [CrossRef]
9. Aaboud, M.; Aad, G.; Abbott, B.; Abeloos, B.; Abidi, S.H.; AbouZeid, O.S.; Abraham, N.L.; Abramowicz, H.; Abreu, H.; Abreu, R.; et al. Search for squarks and gluinos in final states with jets and missing transverse momentum using 36 fb^{-1} of $\sqrt{s} = 13$ TeV pp collision data with the ATLAS detector. *Phys. Rev. D* **2018**, *97*, 112001. [CrossRef]
10. Vami, T.A.; ATLAS; CMS. Searches for gluinos and squarks. In Proceedings of the 7th Large Hadron Collider Physics Conference (LHCP 2019), Puebla, Mexico, 20–25 May 2019; Volume 168. [CrossRef]
11. Sirunyan, A.M.; Tumasyan, A.; Adam, W.; Ambrogi, F.; Asilar, E.; Bergauer, T.; Brandstetter, J.; Brondolin, E.; Dragicevic, M.; Erö, J.; et al. Search for new phenomena with the M_{T2} variable in the all-hadronic final state produced in proton–proton collisions at $\sqrt{s} = 13$ TeV. *Eur. Phys. J. C* **2017**, *77*, 710. [CrossRef]
12. Leggett, T.; Li, T.; Maxin, J.A.; Nanopoulos, D.V.; Walker, J.W. No Naturalness or Fine-tuning Problems from No-Scale Supergravity. *arXiv* **2014**, arXiv:1403.3099.
13. Leggett, T.; Li, T.; Maxin, J.A.; Nanopoulos, D.V.; Walker, J.W. Confronting Electroweak Fine-tuning with No-Scale Supergravity. *Phys. Lett. B* **2015**, *740*, 66. [CrossRef]
14. Du, G.; Li, T.; Nanopoulos, D.V.; Raza, S. Super-Natural MSSM. *Phys. Rev. D* **2015**, *92*, 025038.
15. Cremmer, E.; Ferrara, S.; Kounnas, C.; Nanopoulos, D.V. Naturally Vanishing Cosmological Constant In N = 1 Supergravity. *Phys. Lett. B* **1983**, *133*, 61. [CrossRef]
16. Ellis, J.R.; Lahanas, A.B.; Nanopoulos, D.V.; Tamvakis, K. No-Scale Supersymmetric Standard Model. *Phys. Lett. B* **1984**, *134*, 429.
17. Ellis, J.R.; Kounnas, C.; Nanopoulos, D.V. Phenomenological SU(1,1) Supergravity. *Nucl. Phys. B* **1984**, *241*, 406. [CrossRef]
18. Ellis, J.R.; Kounnas, C.; Nanopoulos, D.V. No Scale Supersymmetric Guts. *Nucl. Phys. B* **1984**, *247*, 373. [CrossRef]
19. Lahanas, A.B.; Nanopoulos, D.V. The Road to No Scale Supergravity. *Phys. Rept.* **1987**, *145*, 1–139. [CrossRef]
20. Giudice, G.F.; Masiero, A. A Natural Solution to the mu Problem in Supergravity Theories. *Phys. Lett. B* **1988**, *206*, 480. [CrossRef]

21. Berkooz, M.; Douglas, M.R.; Leigh, R.G. Branes intersecting at angles. *Nucl. Phys. B* **1996**, *480*, 265. [CrossRef]
22. Ibanez, L.E.; Marchesano, F.; Rabadan, R. Getting just the standard model at intersecting branes. *J. High Energy Phys.* **2001**, *0111*, 2.
23. Blumenhagen, R.; Kors, B.; Lust, D.; Ott, T. The standard model from stable intersecting brane world orbifolds. *Nucl. Phys. B* **2001**, *616*, 3–33.
24. Cvetič, M.; Shiu, G.; Uranga, A.M. Three-family supersymmetric standardlike models from intersecting brane worlds. *Phys. Rev. Lett.* **2001**, *87*, 201801. [CrossRef] [PubMed]
25. Cvetič, M.; Shiu, G.; Uranga, A.M. Chiral four-dimensional N = 1 supersymmetric type IIA orientifolds from intersecting D6-branes. *Nucl. Phys. B* **2001**, *615*, 3. [CrossRef]
26. Cvetič, M.; Papadimitriou, I.; Shiu, G. Supersymmetric three family SU(5) grand unified models from type IIA orientifolds with intersecting D6-branes. *Nucl. Phys. B* **2003**, *659*, 193; Erratum in *Nucl. Phys. B* **2004**, *696*, 298. [CrossRef]
27. Cvetic, M.; Li, T.; Liu, T. Supersymmetric patiSalam models from intersecting D6-branes: A Road to the standard model. *Nucl. Phys. B* **2004**, *698*, 163. [CrossRef]
28. Cvetic, M.; Langacker, P.; Li, T.; Liu, T. D6-brane splitting on type IIA orientifolds. *Nucl. Phys. B* **2005**, *709*, 241. [CrossRef]
29. Cvetic, M.; Li, T.; Liu, T. Standard-like models as type IIB flux vacua. *Phys. Rev. D* **2005**, *71*, 106008. [CrossRef]
30. Chen, C.-M.; Kraniotis, G.V.; Mayes, V.E.; Nanopoulos, D.V.; Walker, J.W. A supersymmetric flipped SU(5) intersecting brane world. *Phys. Lett. B* **2005**, *611*, 156. [CrossRef]
31. Chen, C.-M.; Kraniotis, G.V.; Mayes, V.E.; Nanopoulos, D.V.; Walker, J.W. A K-theory anomaly free supersymmetric flipped SU(5) model from intersecting branes. *Phys. Lett. B* **2005**, *625*, 96. [CrossRef]
32. Chen, C.M.; Li, T.; Nanopoulos, D.V. Standard-like model building on type II orientifolds. *Nucl. Phys. B* **2006**, *732*, 224. [CrossRef]
33. Blumenhagen, R.; Cvetic, M.; Langacker, P.; Shiu, G. Toward realistic intersecting D-brane models. *Ann. Rev. Nucl. Part. Sci.* **2005**, *55*, 71. [CrossRef]
34. Pati, J.C.; Salam, A. Lepton Number as the Fourth Color. *Phys. Rev. D* **1974**, *10*, 275; Erratum in *Phys. Rev. D* **1975**, *11*, 703. [CrossRef]
35. Chen, C.M.; Li, T.; Mayes, V.E.; Nanopoulos, D.V. A Realistic world from intersecting D6-branes. *Phys. Lett. B* **2008**, *665*, 267. [CrossRef]
36. Chen, C.M.; Li, T.; Mayes, V.E.; Nanopoulos, D.V. Towards realistic supersymmetric spectra and Yukawa textures from intersecting branes. *Phys. Rev. D* **2008**, *77*, 125023. [CrossRef]
37. Li, T.; Nanopoulos, D.V.; Raza, S.; Wang, X.C. A Realistic Intersecting D6-Brane Model after the First LHC Run. *J. High Energy Phys.* **2014**, *1408*, 128. [CrossRef]
38. Sabir, M.; Li, T.; Mansha, A.; Wang, X.C. The supersymmetry breaking soft terms, and fermion masses and mixings in the supersymmetric Pati-Salam model from intersecting D6-branes. *J. High Energy Phys.* **2022**, *4*, 89. [CrossRef]
39. Baer, H.; Paige, F.E.; Protopopescu, S.D.; Tata, X. ISAJET 7.48: A Monte Carlo event generator for p p, anti-p p, and e+ e-reactions. *arXiv* **2003**, arXiv:hep-ph/0001086.
40. Tevatron Electroweak Working Group; CDF Collaboration; D0 Collab. Combination of CDF and D0 Results on the Mass of the Top Quark. *arXiv* **2009**, arXiv:0903.2503.
41. Belanger, G.; Boudjema, F.; Pukhov, A.; Singh, R.K. Constraining the MSSM with universal gaugino masses and implication for searches at the LHC. *J. High Energy Phys.* **2009**, *911*, 26. [CrossRef]
42. Baer, H.; Kraml, S.; Sekmen, S.; Summy, H. Dark matter allowed scenarios for Yukawa-unified SO(10) SUSY GUTs. *J. High Energy Phys.* **2008**, *803*, 56. [CrossRef]
43. Patrignani, C.; Agashe, K.; Aielli, G.; Amsler, C.; Antonelli, M.; Asner, D.M.; Baer, H.; Banerjee, S.; Barnett, R.M.; Basaglia, T.; et al. Review of Particle Physics. *Chin. Phys. C* **2016**, *40*, 100001.
44. Aad, G.; Abbott, B.; Abbott, D.C.; Abud, A.A.; Abeling, K.; Abhayasinghe, D.K.; Abidi, S.H.; AbouZeid, O.S.; Abraham, N.L.; Abramowicz, H.; et al. Measurements of the Higgs boson production and decay rates and constraints on its couplings from a combined ATLAS and CMS analysis of the LHC pp collision data at $\sqrt{s} = 7$ and 8 TeV. *J. High Energy Phys.* **2016**, *1608*, 45.
45. Slavich, P.; Heinemeyer, S.; Bagnaschi, E.; Bahl, H.; Goodsell, M.; Haber, H.E.; Hahn, T.; Harlander, R.; Hollik, W.; Lee, G.; et al. Higgs-mass predictions in the MSSM and beyond. *Eur. Phys. J. C* **2021**, *81*, 450. [CrossRef]
46. Allanach, B.C.; Djouadi, A.; Kneur, J.L.; Porod, W.; Slavich, P. Precise determination of the neutral Higgs boson masses in the MSSM. *J. High Energy Phys.* **2004**, *9*, 44. [CrossRef]
47. Baer, H.; Brhlik, M. Signals for the minimal gauge-mediated supersymmetry-breaking model at the Fermilab Tevatron collider. *Phys. Rev. D* **1997**, *55*, 4463. [CrossRef]
48. Baer, H.; Brhlik, M.; Castano, D.; Tata, X. b→ s γconstraints on the minimal supergravity model with large tan β. *Phys. Rev. D* **1998**, *58*, 015007. [CrossRef]
49. Babu, K.; Kolda, C. Higgs-mediated $B^0 \to \mu^+\mu^-$ in minimal supersymmetry. *Phys. Rev. Lett.* **2000**, *84*, 228. [CrossRef] [PubMed]
50. Dedes, A.; Dreiner, H.; Nierste, U. Correlation of $B_s \to \mu^+\mu^-$ and $(g-2)\mu$ in minimal supergravity. *Phys. Rev. Lett.* **2001**, *87*, 251804. [CrossRef] [PubMed]
51. Mizukoshi, J.K.; Tata, X.; Wang, Y. Higgs-mediated leptonic decays of B_s and B_d mesons as probes of supersymmetry. *Phys. Rev. D* **2002**, *66*, 115003. [CrossRef]
52. Khachatryan, V.; Sirunyan, A.M.; Tumasyan, A.; Adam, W.; Bergauer, T.; Filipovic, N.; Bencze, G.; Hajdu, C.; Hidas, P.; Horváth, D.; et al. Observation of the rare $B_s^0 \to \mu^+\mu^-$ decay from the combined analysis of CMS and LHCb data. *Nature* **2015**, *522*, 68.

53. Amhis, Y.; Banerjee, S.; Ben-Haim, E.; Blyth, S.; Bozek, A.; Bozzi, C.; Carbone, A.; Chistov, R.; Chrząszcz, M.; Cibinetto, G.; et al. Averages of *b*-hadron, *c*-hadron, and τ-lepton properties as of summer 2014. *arXiv* **2014**, arXiv:1412.7515.

54. Aghanim, N.; Akrami, Y.; Arroja, F.; Ashdown, M.; Aumont, J.; Baccigalupi, C.; Ballardini, M.; Banday, A.J.; Barreiro, R.B.; Bartolo, N.; et al. Planck 2018 results. I. Overview and the cosmological legacy of Planck. *Astron. Astrophys.* **2020**, *641*, A1. [CrossRef]

55. Cohen, T.; Golling, T.; Hance, M.; Henrichs, A.; Howe, K.; Loyal, J.; Padhi, S.; Wacker, J.G. SUSY Simplified Models at 14, 33, and 100 TeV Proton Colliders. *J. High Energy Phys.* **2014**, *4*, 117. [CrossRef]

56. Arkani-Hamed, N.; Han, T.; Mangano, M.; Wang, L.T. Physics opportunities of a 100 TeV proton–proton collider. *Phys. Rept.* **2016**, *652*, 1–49. [CrossRef]

57. Fan, J.; Jaiswal, P.; Leung, S.C. Jet Observables and Stops at 100 TeV Collider. *Phys. Rev. D* **2017**, *96*, 036017. [CrossRef]

58. Golling, T.; Hance, M.; Harris, P.; Mangano, M.L.; McCullough, M.; Moortgat, F.; Schwaller, P.; Torre, R.; Agrawal, P.; Alves, D.S.M.; et al. Physics at a 100 TeV pp collider: Beyond the Standard Model phenomena. *arXiv* **2016**, arXiv:1606.00947. [CrossRef]

59. Tumasyan, A.; Adam, W.; Andrejkovic, J.W.; Bergauer, T.; Chatterjee, S.; Damanakis, K.; Dragicevic, M.; Del Valle, A.E.; Fruehwirth, R.; Jeitler, M.; et al. Searches for additional Higgs bosons and for vector leptoquarks in $\tau\tau$ final states in proton-proton collisions at $\sqrt{s}$ = 13 TeV. *arXiv* **2022**, arXiv:2208.02717.

60. Baer, H.; Barger, V.; Tata, X.; Zhang, K. Prospects for Heavy Neutral SUSY HIGGS Scalars in the hMSSM and Natural SUSY at LHC Upgrades. *Symmetry* **2022**, *14*, 2061. [CrossRef]

61. Baer, H.; Barger, V.; Tata, X.; Zhang, K. Detecting heavy neutral SUSY Higgs bosons decaying to sparticles at the high-luminosity LHC. *arXiv* **2022**, arXiv:2212.09198.

62. [ATLAS]. SUSY Summary Plots June 2021. ATL-PHYS-PUB-2021-019. Available online: https://cds.cern.ch/record/2771785/files/ATL-PHYS-PUB-2021-019.pdf (accessed on 25 February 2024).

63. Tumasyan, A.; Adam, W.; Andrejkovic, J.W.; Bergauer, T.; Chatterjee, S.; Damanakis, K.; Dragicevic, M.; Escalante Del Valle, A.; Fruehwirth, R.; Jeitler, M.; et al. Search for direct pair production of supersymmetric partners of τ leptons in the final state with two hadronically decaying τ leptons and missing transverse momentum in proton-proton collisions at $\sqrt{s}$ = 13 TeV. *arXiv* **2022**, arXiv:2207.02254.

64. Aad, G.; Abbott, B.; Abbott, D.C.; Abud, A.A.; Abeling, K.; Abhayasinghe, D.K.; Abidi, S.H.; AbouZeid, O.S.; Abraham, N.L.; Abramowicz, H.; et al. Search for new phenomena in events with an energetic jet and missing transverse momentum in *pp* collisions at $\sqrt{s}$ =13 TeV with the ATLAS detector. *Phys. Rev. D* **2021**, *103*, 112006.

65. [ATLAS]. SUSY March 2023 Summary Plot Update. ATL-PHYS-PUB-2023-005. Available online: https://atlas.web.cern.ch/Atlas/GROUPS/PHYSICS/PUBNOTES/ATL-PHYS-PUB-2023-005/ (accessed on 25 February 2024).

66. Akerib, D.S.; Alsum, S.; Araújo, H.M.; Bai, X.; Bailey, A.J.; Balajthy, J.; Beltrame, P.; Bernard, E.P.; Bernstein, A.; Biesiadzinski, T.P.; et al. Results from a search for dark matter in the complete LUX exposure. *Phys. Rev. Lett.* **2017**, *118*, 021303. [CrossRef] [PubMed]

67. Aprile, E.; Aalbers, J.; Agostini, F.; Alfonsi, M.; Amaro, F.D.; Anthony, M.; Arneodo, F.; Barrow, P.; Baudis, L.; Bauermeister, B.; et al. First Dark Matter Search Results from the XENON1T Experiment. *Phys. Rev. Lett.* **2017**, *119*, 181301. [CrossRef] [PubMed]

68. Collaboration, X.E.N.O.N.; Aprile, E.; Aalbers, J.; Agostini, F.; Alfonsi, M.; Althueser, L.; Amaro, F.D.; Anthony, M.; Arneodo, F.; Baudis, L.; et al. Dark Matter Search Results from a One Ton-Year Exposure of XENON1T. *Phys. Rev. Lett.* **2018**, *121*, 111302.

69. Aprile, E.; Aalbers, J.; Agostini, F.; Alfonsi, M.; Amaro, F.D.; Anthony, M.; Arazi, L.; Arneodo, F.; Balan, C.; Barrow, P.; et al. Physics reach of the XENON1T dark matter experiment. *J. Cosmol. Astropart. Phys.* **2016**, *1604*, 27. [CrossRef]

70. Akerib, D.S.; Alsum, S.; Araújo, H.M.; Bai, X.; Bailey, A.J.; Balajthy, J.; Beltrame, P.; Bernard, E.P.; Bernstein, A.; Biesiadzinski, T.P.; et al. Limits on spin-dependent WIMP-nucleon cross section obtained from the complete LUX exposure. *Phys. Rev. Lett.* **2017**, *118*, 251302. [CrossRef] [PubMed]

71. Akerib, D.S.; Araújo, H.M.; Bai, X.; Bailey, A.J.; Balajthy, J.; Beltrame, P.; Bernard, E.P.; Bernstein, A.; Biesiadzinski, T.P.; Boulton, E.M.; et al. Results on the Spin-Dependent Scattering of Weakly Interacting Massive Particles on Nucleons from the Run 3 Data of the LUX Experiment. *Phys. Rev. Lett.* **2016**, *116*, 161302. [CrossRef]

72. Abbasi, R.; Abdou, Y.; Ackermann, M.; Adams, J.; Ahlers, M.; Andeen, K.; Auffenberg, J.; Bai, X.; Baker, M.; Barwick, S.W.; et al. Limits on a muon flux from neutralino annihilations in the Sun with the IceCube 22-string detector. *Phys. Rev. Lett.* **2009**, *102*, 201302. [CrossRef]